P247 EVALUATING THE IMPACTS OF NASA/SPORT DAILY GREENNESS VEGETATION FRACTION ON LAND SURFACE MODEL AND NUMERICAL WEATHER FORECASTS

Jordan R. Bell[1], Jonathan L. Case[2], Frank J. LaFontaine[3], and Sujay V. Kumar[4]

[1]University of Missouri-Atmospheric Science, Columbia, MO
[2]ENSCO, Inc./Short-term Prediction Research and Transition (SPoRT) Center, Huntsville, AL
[3]Raytheon/SPoRT Center, Huntsville, AL
[4]SAIC/NASA Goddard Space Flight Center, Greenbelt, MD

1. INTRODUCTION

A key ingredient in the development of convection is surface heating and moisture transport into the atmosphere. An important mechanism of moisture transport is evapotranspiration, especially during the warm season. Healthy, full vegetation leads to higher evapotranspiration rates and therefore, an increase in the amount of moisture available in the atmosphere. One variable that represents the coverage and health of the vegetation in weather models is the Greenness Vegetation Fraction (GVF). GVF values can be derived through remote-sensing techniques using polar-orbiting satellites.

The NASA Short-term Prediction Research and Transition (SPoRT) Center has developed a real-time, high-resolution GVF product for use in weather prediction models. The objective of the SPoRT Center is to transition unique NASA observations and research capabilities to the operational weather community to improve short-term forecasts. SPoRT developed this NASA GVF product to improve the representation of vegetation in weather models over the current operational GVF dataset, a ~20-year-old dataset that remains static from year to year. The static dataset currently used in operational and research community models may not properly represent the vegetation patterns of the United States in regions that have changed over the last two decades through urbanization, or experienced substantial deviations from climatology (e.g. droughts, excessive rainfall, late/early season freezes or blooms). Recent research has demonstrated that a real-time satellite product, like the SPoRT GVF, has the capability to improve weather model accuracy (Kurkowski and Stensrud 2003; James et al. 2009).

The goal of this summer internship was to compare the SPoRT GVF dataset to the current GVF static dataset, or "climatology", and to assess the impacts on land surface and weather prediction models. The project had two specific objectives. The first was to compare the SPoRT GVF dataset to the National Centers for Environmental Prediction (NCEP) climatology GVF during June to October 2010. This part of the project was employed to see how the SPoRT data set impacted a land surface model apart from a full numerical weather prediction (NWP) model. The second phase focused on the impact of the SPoRT GVF on an NWP model, specifically the Weather Research and Forecasting (WRF) model. A severe weather case study from 2010 was chosen and then two WRF simulations, one with each dataset, were run and their differences examined.

The remainder of this paper is organized as follows. Section 2 provides a description of the two GVF datasets being compared. Section 3 discusses the methodology employed for the analysis. Results are then presented in Section 4, followed by summary/conclusions in Section 5. Acknowledgements/Disclaimer and References are in Sections 6 and 7, respectively

*Corresponding author address: Jonathan Case, ENSCO, Inc., 320 Sparkman Dr., Room 3062, Huntsville, AL, 35805. Email: Jonathan.Case-1@nasa.gov

2. DESCRIPTION OF GVF DATASETS

2.1 NCEP Climatology GVF

The GVF dataset used in current national operational weather models is a monthly climatology derived from the Normalized Difference Vegetation Index (NDVI) from the Advanced Very High Resolution Radiometer (AVHRR) aboard NOAA polar-orbiting satellites. The GVF climatology was produced at 0.144° resolution using 5 years of AVHRR NDVI data (1985-1991; Gutman and Ignatov 1998; Jiang et al. 2010). Representing data at the mid-point of every month, this dataset has been implemented into the operational Noah land surface model (LSM) at NCEP and within the WRF model (Ek et al. 2003; Jiang et al. 2010; Skamarock et al. 2008). It should be noted that a newer 24-year AVHRR GVF climatology was presented by Jiang et al. 2010, along with a near real-time weekly GVF dataset. As of this writing, it is not currently known when this new database will be implemented into operational weather models at NCEP.

Because the current GVF climatology is static from year to year, this can present a problem as the actual vegetation may not be the same as depicted by the climatology. The NCEP GVF cannot take into account how vegetation may respond to anomalous weather conditions, such as hard freezes, droughts, and extreme temperature/precipitation anomalies. The current operational GVF also does not take into account some urban areas that have changed drastically since the climatology was compiled. In addition, its coarse resolution of 0.144° cannot adequately resolve large variations in vegetation coverage over small distances, such as in regions of

complex terrain (e.g. Rocky Mountains) or urban/suburban regions.

2.2 SPoRT GVF

The NASA SPoRT Center has developed a real-time GVF product for NWP models that has the potential to help improve the accuracy of these models. The SPoRT GVF is updated daily based on 1-km resolution NDVI swath data taken from the Moderate Resolution Imaging Sprectroradiometer (MODIS) aboard the NASA Aqua and Terra polar-orbiting satellites. The SPoRT GVF data have been produced daily on a Continental U.S. (CONUS) grid since 1 June 2010. The NDVI is calculated using the near-IR and visible (red) wavelengths of the MODIS sensor, and is defined as:

$$NDVI = \frac{\rho_{NIR} - \rho_{RED}}{\rho_{NIR} + \rho_{RED}} \quad (1),$$

where ρ_{NIR} is the reflectance of the near-IR wavelengths (0.75–1.5 μm) and the ρ_{RED} is the reflectance on the visible red channel (0.6–0.7 μm). The raw NDVI ranges from -1 to +1, with larger values closer to +1 indicative of a full coverage of healthy vegetation. Values near 0 indicate little to no vegetation present, while values below 0 tend to indicated snow or ice cover.

The NDVI used in SPoRT's product is first projected to a 0.01° (~1 km) grid. Since the data come from polar-orbiting satellites, not all the pixels are sampled daily. Therefore, a time-weighting algorithm is applied to the NDVI data when creating a composite over the CONUS. This algorithm queries the previous 20 days for up to six pieces of NDVI data to ensure a near fully-populated grid, using the following formula at each grid point (Case et al. 2011):

$$NDVI(j,i) = \begin{cases} \dfrac{\sum_{n=1}^{m} NDVI_n \left(\dfrac{1.0}{DaysLate_n + 1} \right)}{\left(\dfrac{1.0}{DaysLate_n + 1} \right)} ; m \geq 1 \\ \text{where } m = \#\text{ of NDVIvalues at } (j,i) \\ -9.999 \text{ (missing)} ; m = 0 \end{cases} \quad (2).$$

The SPoRT GVF is calculated on the same 0.01° grid using the procedure outlined in Zeng et al. (2000) and Miller et al. (2006), which utilized at least a year's worth of NDVI data in the computations of GVF. Since the SPoRT GVF dataset did not have a full year's worth of NDVI data for the period of study, maximum values of NDVI at each grid point ($NDVI_{max}$) were calculated using the June through October data. Upon finding the $NDVI_{max}$ at each pixel, they are then sorted by land-use class and grouped together into single histogram distributions. The $NDVI_{max}$ values are then sorted in order to find the 90th percentile for each land-use class ($NDVI_{V,i}$), and the 5th percentile for the barren land class ($NDVI_S$). The GVF is then computed using the following formula:

$$GVF_i = \frac{NDVI_i - NDVI_S}{NDVI_{V,i} - NDVI_S} \quad (3),$$

where $NDVI_i$ is the actual real-time NDVI value at a given pixel, $NDVI_s$ is a global constant that represents the 5th percentile of the $NDVI_{max}$ values for the barren vegetation class, and $NDVI_{V,i}$ is the 90th percentile of $NDVI_{max}$ for the vegetation class at grid point *i* (Case et al. 2011). The GVF is bounded between 0 and 1 to ensure a realistic range of values. It should be noted that no corrections are made to the NDVI swath data due to viewing angle differences of the satellite. Missing data at any grid points are then filled with the NCEP GVF monthly climatology, time-interpolated to the current day.

When comparing the two datasets to each other, it is apparent how much more detail is resolved by the SPoRT GVF. The NCEP GVF interpolated linearly in time to 17 July (Figure 1a) depicts a much smoother field compared to the 1-km resolution SPoRT-MODIS composite from 17 July (Figure 1b). Also, many portions of the western half of the domain experience an increase in GVF over the NCEP dataset, up to 40% in some instances, particularly over the High Plains (Figure 1c). A likely factor contributing to these widespread positive differences in the SPoRT GVF dataset relative to the NCEP climatology is that the precipitation in the late Spring and early Summer was much above average all along the High Plains region (Figure 2). Another possible reason for the higher SPoRT GVF in the intermountain west is the increased resolution of the product itself. The SPoRT GVF product has approximately 15 times finer resolution than the NCEP climatology and therefore is able to resolve the complex terrain features much better (e.g. Sierra Nevada range in eastern California).

3. METHODOLOGY

To examine the impacts of using the daily SPoRT versus the monthly NCEP climatology GVFs, statistics of the Noah LSM were produced during the 2010 warm season, as run within the NASA Land Information System (LIS). The NASA LIS is a high performance land surface modeling and data assimilation system that integrates satellite-derived datasets, ground-based observations and model reanalyses to force a variety of LSMs (Kumar et al. 2006, 2007). In this study, the operational Noah LSM is invoked within LIS to produce model runs using the NCEP and SPoRT GVFs. The second component of this study involves generating control and experimental WRF simulations that use the NCEP climatology and SPoRT GVFs, respectively. The next two sub-sections describe in more detail the experiment design for each component of this research.

3.1 LIS-Noah Runs during 2010 Warm Season

The LIS-Noah runs to generate comparison statistics were conducted in an "offline" mode, in which the Noah LSM is integrated apart from a full NWP model. A domain with 1-km grid spacing was employed to cover the entire CONUS and adjacent portions of Mexico and Canada, closely paralleling the

domain of the SPoRT GVF composites. The domain was then decomposed into four quadrants (Figure 1c) to examine GVF and LSM statistics in the different regions. In the offline integration, global atmospheric analyses from the NCEP Global Forecast System (GFS) Data Assimilation System (GDAS; Derber et al. 1991) were used to drive the integration of land surface variables within LIS-Noah (e.g. soil moisture, soil temperature, sensible and latent heat flux, etc.).

The offline LIS run was cold-started on 1 June 2008 with a uniform first-guess soil temperature and volumetric soil moisture of 290 K and 25%, respectively, in all soil layers. The Noah LSM was integrated for a time period of 2 years to 1 June 2010, using a time step of 30 minutes. A sufficiently long integration time, or "spin-up", is necessary to ensure that the model states can reach a fine-scale equilibrium with the forcing meteorology (Cosgrove et al. 2003; Rodell et al. 2005). During the two-year spin-up integration, the NCEP GVF climatology was used. After 0000 UTC 1 June 2010, the spin-up run was re-started for two separate offline integrations, a control run that continued using the NCEP GVFs, and an experimental run that employed the daily SPoRT GVFs during the period of study from 1 June to 0000 UTC 1 November 2010. Figure 3 portrays a graphic that summarizes the offline LIS methodology.

3.2 Numerical Weather Prediction Case Studies

To examine the potential improvements of the daily SPoRT GVFs on an NWP model, a severe weather event over the Upper Midwest from 17 July was analyzed in a sensitivity case study. This event was chosen because of its relatively pristine surface heating during much of the day preceding the onset of severe convection. The Advanced Research WRF (ARW; Skamarock et al. 2008) model coupled to the NASA LIS was used as the vehicle for conducting the sensitivity simulations. First, a separate offline LIS-Noah simulation was conducted with 4-km horizontal grid spacing over a CONUS domain identical to the real-time WRF model configuration run at the National Severe Storms Laboratory that provides additional severe weather forecasts guidance to the Storm Prediction Center (Kain et al. 2010). This LIS-Noah offline run was done with the same initial cold start and spin-up time window as described above (1 June 2008 to 1 June 2010). Additionally, beginning at 0000 UTC 1 June 2010, two separate offline LIS re-start runs were made on this 4-km domain, one continuing to use the NCEP GVF climatology with the other incorporating the daily SPoRT GVFs from 1 June to 1 November.

Second, coupled LIS/ARW simulations were run out to 36 hours, initialized at 0000 UTC 17 July. Two coupled simulations were initialized using the different GVFs and offline LIS runs valid at the model start time (Figure 3). The outputs of the two different runs were then compared and analyzed to check for possible improvements due to the SPoRT GVF. Surface statistical verification was also conducted for additional analysis.

4. RESULTS

4.1 Analysis of LIS-Noah Offline Runs

Figure 4 shows a comparison of the SPoRT and NCEP climatology GVF datasets broken up into four regions as indicated in Figure 1c. The SPoRT GVF values were on average higher than the NCEP climatology in the Western half of the domain. The northeast quadrant's SPoRT GVF means were slightly below the NCEP climatology during July and August, then transitioned to higher GVFs by late Summer and Autumn. There were no obvious weather anomalies in the Northeast associated with the lower Summer GVFs; however, the Autumn featured well above average temperatures across much of the Eastern U.S. (Figure 5), which likely caused the slower decline in the real-time SPoRT GVFs relative to the NCEP climatology. The SPoRT GVFs remained the closest to the climatology in the Southeast quadrant during most of the period of record. Like the Northeast quadrant it was not until late in the warm season when the SPoRT GVFs became consistently higher than the NCEP climatology. The Southeastern quadrant also experienced the "noisiest" day-to-day variations in the SPoRT GVF, especially in September and October. This might be attributed to how the NDVI data were composited onto the grid without any sophisticated viewing angle corrections, representing one of the limitations of the SPoRT product.

The differences in the GVF datasets had a direct impact on the surface fluxes and soil moisture output from the offline Noah LSM integration within LIS. During the time periods when the SPoRT GVF was higher than the NCEP climatology, the 3-hourly averaged latent heat fluxes during the approximate peak daytime heating (i.e. 1800 to 2100 UTC, red lines in Figure 6) increased by up to 30 W m^{-2}, especially in the western half of the domain. The increase in the latent heat flux results from the additional evapotranspiration due to the higher coverage of healthy vegetation.

According to the surface energy balance equation:

$$R_{net}+Q_h+Q_{ls}+Q_g = 0 \qquad (4),$$

the net incoming radiation at the surface (R_{net}) is equally balanced by the sensible heat flux (Q_h), latent heat flux (Q_{le}), and heat flux into the ground (Q_g). Assuming negligible changes in albedo and all other factors being the same (i.e. atmospheric forcing for the LIS-Noah LSM integration does not change between the SPoRT GVF and NCEP GVF model runs), an increase in latent heat flux needs to be off-set by a corresponding decrease in sensible heat flux and/or ground heat flux directed into the soil. While the ground heat flux decreased noticeably in the West with the addition of the SPoRT GVF (not shown), the sensible heat flux decreased the most during the daytime hours (Figure 7).

The increase in latent heat flux in the western half of the domain had the most substantial impact on the volumetric soil moisture. Figure 8 shows the top three layers of mean volumetric soil moisture, and how they

responded to the difference in GVFs. The soil dried out more quickly in the LIS-Noah run using SPoRT GVFs compared to the NCEP climatology, with volumetric soil moisture decreasing as much as 0.015 (1.5%) or more. This more rapid soil drying is a result of the increased latent heat flux (and evapotranspiration) caused by the higher vegetation coverage, thereby extracting moisture more quickly from the soil, particularly in the root zone layers of 10–40 cm and 40–100 cm. The eastern half of the domain experienced only marginal changes in volumetric soil moisture, generally less than 0.5% by the end of the warm season.

The most intriguing result of the offline LIS-Noah analysis was in the two western quadrants towards the end of the warm season. The latent heat flux remained higher during the whole period of record because of the increase in the mean GVF (Figure 6a, c). However, by mid-summer, the sensible heat flux differences transitioned from negative to positive, and remained consistently positive for the remainder of the study period (Figure 7a, c). Typically these two fluxes are approximately the inverse of one other. However, the drier soil over the western portion of the domain in the SPoRT GVF run enabled a slight increase in the sensible heat flux since less energy was required to evaporate moisture from the soil medium. Consequently, skin temperature increased slightly in the SPoRT GVF run by late summer (not shown), producing the increases in sensible heat flux.

4.2 WRF Model Case Study

4.2.1 **17 July 2010 Severe Weather event**

The 1200 UTC surface map (Figure 9a) provides a background on this event. A warm front was positioned over southwestern Minnesota and a cold front was situated over the western Dakotas. As the warm front lifted to the northeast, the warm sector cleared out allowing for optimal daytime heating to impact the surface. The eastward-advanced cold front provided the forcing for the outbreak to occur. The Storms Prediction Center had a total of 369 storm reports on this day, with the majority of the reports comes from Minnesota and Iowa (Figure 9b). This day was chosen because it experienced the full effect of the daytime peak heating on varying GVFs.

Figure 10 depicts the two GVF products and the differences over the Upper Midwest focus area (hereafter referred to as the domain). In the western portion of the domain, the SPoRT GVF is 20–40% higher in many places. Meanwhile, in the northeastern and southeastern portions of the domain, the SPoRT GVF was about 10–20% lower than the NCEP climatology. The central portion of the domain where the majority storm reports occurred did not experience much change in GVF.

The forecast 2-m temperatures shows that the control WRF run using the NCEP GVF data (Figure 11a) has a larger area of 36–39°C temperatures at 21 hours compared to the WRF run using the SPoRT GVF data (Figure 11b). The control run also has a pocket of 2-m temperatures exceeding 39°C in South Dakota not found in the SPoRT run. Observations from that same time period (Figure 11d) show that the SPoRT run is more consistent with observed reports over portions of South Dakota while the control run is too warm. The northeastern part of the domain where the SPoRT GVF was lower than the NCEP climatology shows an increase in temperature of 0.5–2°C in some areas (Figure 11c).

The increase in the SPoRT GVF on the western side of the domain also impacted the simulated 2-m dewpoint. Figure 12 shows the 21-h forecast 2-m dewpoint, the difference, and the 2100 UTC observations. Since higher GVFs lead to an increase in latent heat flux, the larger SPoRT GVF over the Dakotas and Nebraska resulted in 2-m dewpoint rises of 2–4°C or higher (Figure 12c). The areas of lower SPoRT GVF experienced a similar decline in 2-m dewpoints. The higher 2-m dewpoint in the SPoRT run resulted in higher Convective Available Potential Energy (CAPE) values up to 500–1000 J kg^{-1} over the regions with the higher SPoRT GVF (Figure 13). The higher CAPE air was upstream of the region where convection initiated late in the day, thus impacting the evolution of forecast precipitation.

In terms of the simulation precipitation, the two model runs initially had small differences, but these variations increased with time. In the 27-h forecast (Figure 14), both the control and SPoRT runs depict a band of convection in roughly the same area with embedded heavier storms over southern Minnesota. The control run simulated the convection in more of a continuous line with a bowing look to it (Figure 14a), while the SPoRT run suggested a slightly more discrete mode (Figure 14b-c). Neither model run, however, depicted the convective mode as discrete as the validating stage IV analysis (Figure 14d).

By the 34-h forecast, the differences between the model runs are more substantial. The control run rapidly advanced the precipitation into northeastern Missouri, while the SPoRT run still had the bulk of the precipitation in southern Iowa (Figure 15). The SPoRT run compares more favorably to the actual observation on placement as well as intensity (Figure 15b, d). Both model runs, however, missed the precipitation that occurred at this time in northern Wisconsin.

4.2.2 **Surface Verification**

The Model Evaluation Tools (MET; Brown et al. 2009) package was employed to produce model verification statistics at surface observation locations in both WRF forecasts. The Northern Plains (NPL) and Midwest (MDW) regions from the NCEP verification regions map (Figure 16) were chosen because both fall within the focus domain investigated.

The mean error for 2-m temperature and 2-m dewpoint from the 17 July model runs is given in Figure 17. In the NPL region where the SPoRT GVFs were considerably larger than the NCEP GVFs, the SPoRT-WRF had a 2-m temperature bias that was consistently 1–1.5°C lower than the NCEP-WRF bias, which particularly became prevalent during daytime heating period (forecast hours 12–24 in Figure 17a). Both model configurations experienced the lowest bias in 2-m temperature during forecast hours 24 and 25. The model biases do not show much difference in MDW

because of the small differences in GVF; however, the model biases do vary from -1°C to -3° during the course of the forecast period, indicative of a consistent cold bias both day and night that may not necessarily be related to land surface impacts.

The mean error in 2-m dewpoint in the NPL region also experiences rather large differences. The higher GVFs in the SPoRT-WRF run resulted in an overall higher bias, with nearly a 2°C increase over the NCEP-WRF run during the hours of daytime heating (Figure 17b). This adjustment in the mean 2-m dewpoint acted to correct (and in some cases, over-correct) a persistent dry bias in the NCEP-WRF run. The bias trends over the MDW region closely resemble that of the NPL region, but with very little differences between the NCEP and SPoRT model runs.

The error standard deviation (ESD), which measures the random errors in the model, was also examined as part of the verification (Figure 18). In the NPL region, there were larger ESDs during the nighttime (forecast hours 0–12 and 24–36 in Figure 18a) in both model runs compared to the MDW region. After experiencing the effects of daytime heating, the NCEP-WRF has slightly higher ESD than the SPoRT WRF by about 0.3°C. The errors tend to be much more similar in MDW than in NPL, which is consistent with the largest GVF differences being over the NPL region. The NPL region also has the largest differences in 2-m dewpoint ESD. The daytime error is larger by a few tenths of a degree in the NCEP-WRF, while the nighttime ESD is slightly larger in the SPoRT-WRF results (Figure 18b).

Finally, the precipitation verification revealed some improvements in the SPoRT-WRF run in this case. The Critical Success Index (CSI, also known as the threat score for precipitation) represents the ratio of the number of times an event was correctly forecast to the number of times it was either forecast or occurred. Ranging from 0 (no skill) to 1 (perfect forecast), the CSI ignores correct rejection forecasts, thus making it an appropriate statistic for examining precipitation verification because of its low areal coverage.

Figure 19 shows the CSI scores as a function of forecast hour for the 1-mm h^{-1} accumulated precipitation. Only the MDW region is presented due to the majority of the precipitation falling within this region on 17–18 July. The CSI peaks in both model runs near 0.4 around 24–28 h, with slightly higher values in the SPoRT-WRF run. The most noteworthy difference is that the SPoRT-WRF has a higher CSI (+0.1) between forecast hours 32 and 36. This is a result of the SPoRT-WRF having a better agreement with the observed nocturnal precipitation over Iowa, whereas the convection moved into Missouri too quickly in the NCEP-WRF run.

5. SUMMARY AND CONCLUSIONS

This paper presented a comparison of a new, high-resolution NASA GVF dataset produced in real time to the current NCEP operational GVF static climatology. The evaluation of the SPoRT-MODIS GVF revealed some improvements over using the climatology GVF. The SPoRT dataset was able to depict the impacts of above-average precipitation, manifested in larger GVF values over the High Plains of the United States. The higher GVFs in the western United States initially resulted in higher (lower) latent (sensible) heat fluxes. However, by the end of the 2010 warm season both fluxes were higher, because of the increased evapotranspiration causing the soil moisture to dry out more quickly. The SPoRT dataset was also able to show the vegetation's response to the above-average temperatures in the eastern United States during late summer and early fall, resulting in substantial deviations from the NCEP climatological GVF by the Autumn months.

By examining the SPoRT GVF impacts on an NWP case study, a couple of key results were noted. First, areas that had experienced higher (lower) GVF values saw an increase (decrease) in the simulated 2-m dewpoints (temperatures). The increase in moisture led to higher forecast CAPE values over the NPL region, which played a role in the intensity, evolution, and mode of simulated convection. These alternations in the predicted surface fields led to some improvements in the location and timing of simulated precipitation, which correlated better with observations in the SPoRT-WRF run.

This project only focused on the 2010 warm season and one severe weather outbreak. Similar work needs to be done over longer time periods and various seasons. Additional severe weather outbreaks need to be examined, from various areas on the CONUS, in order to fully understand the effects of a real-time GVF dataset. The vegetation patterns of the United States can vary greatly from year to year. By utilizing a real-time GVF product, NWP models can resolve these changes relative to a vegetation climatology, thereby improving the representation of heat and moisture exchanges between the land surface and atmosphere.

6. ACKNOWLEDGEMENTS/DISCLAIMER

Mr. Bell would like to thank the Missouri Space Grant for funding the internship that enabled him to work with the SPoRT Center on this research. Mr. Bell also thanks all the members of the SPoRT Center for their assistance during this project. Computational resources for this work were provided by the NASA Center for Computational Sciences at the NASA Goddard Space Flight Center. Mention of a copyrighted, trademarked or proprietary product, service, or document does not constitute endorsement thereof by the authors, the University of Missouri, ENSCO Inc., Raytheon, SAIC, the SPoRT Center, the National Aeronautics and Space Administration, or the United States Government. Any such mention is solely for the purpose of fully informing the reader of the resources used to conduct the work reported herein.

7. REFERENCES

Brown, B. G., J. H. Gotway, R. Bullock, E. Gilleland, T. Fowler, D. Ahijevych, and T. Jensen, 2009: The Model Evaluation Tools (MET): Community tools for forecast evaluation. Preprints, *25th Conf. on*

International Interactive Information and Processing Systems (IIPS) for Meteorology, Oceanography, and Hydrology, Phoenix, AZ, Amer. Meteor. Soc., 9A.6. [Available online at http://ams.confex.com/ams/pdfpapers/151349.pdf]

Case, J. L., F. J. LaFontaine, S. V. Kumar, and G. J. Jedlovec, 2011: A real-time MODIS vegetation composite for land surface models and short-term forecasting. Preprints, *15th Symp. on Integrated Observing and Assimilation Systems for the Atmosphere, Oceans, and Land Surface,* 11.2.

Cosgrove, B. A., and Coauthors, 2003: Land surface model spin-up behavior in the North American Land Data Assimilation System (NLDAS). *J. Geophys. Res.,* **108(D22),** 8845, doi:10.1029/2002JD003316.

Derber, J. C., D. F. Parrish, and S. J. Lord, 1991: The new global operational analysis system at the National Meteorological Center. *Wea. Forecasting,* **6,** 538-547.

Ek, M. B., K. E. Mitchell, Y. Lin, E. Rogers, P. Grunmann, V. Koren, G. Gayno, and J. D. Tarpley, 2003: Implementation of Noah land surface model advances in the National Centers for Environmental Prediction operational mesoscale Eta model. *J. Geophys. Res.,* **108 (D22),** 8851, doi:10.1029/2002JD003296.

Gutman, G. and A. Ignatov, 1998: Derivation of green vegetation fraction from NOAA/AVHRR for use in numerical weather prediction models. *Int. J. Remote Sensing,* **19,** 1533-1543.

James, K. A., D. J. Stensrud, and N. Yussouf, 2009: Value of real-time vegetation fraction to forecasts of severe convection in high-resolution models. *Wea. Forecasting,* **24,** 187-210.

Jiang, L., and Coauthors, 2010: Real-time weekly global green vegetation fraction derived from advanced very high resolution radiometer-based NOAA operational global vegetation index (GVI) system. *J. Geophys. Res.,* **115,** D11114, doi:10.1029/2009JD013204.

Kain, J. S., S. R. Dembek, S. J. Weiss, J. L. Case, J. J. Levitt, and R. A. Sobash, 2010: Extracting unique information from high-resolution forecast models: Monitoring selected fields and phenomena every time step. *Wea. Forecasting,* **25,** 1536-1542.

Kumar, S. V., and Coauthors, 2006. Land Information System – An Interoperable Framework for High Resolution Land Surface Modeling. *Environmental Modeling & Software,* **21 (10),** 1402-1415, doi:10.1016/j.envsoft.2005.07.004.

Kumar, S. V., C. D. Peters-Lidard, J. L. Eastman, and W.-K. Tao, 2007: An integrated high-resolution hydrometeorological modeling testbed using LIS and WRF. *Environmental Modeling & Software,* **23 (2),** 169-181, doi: 10.1016/j.envsoft.2007.05.012.

Kurkowski, N. P., D. J. Stensrud, and M. E. Baldwin, 2003: Assessment of implementing satellite-derived land cover data in the Eta model. *Wea. Forecasting,* **18,** 404-416.

Rodell, M., P. R. Houser, A. A. Berg, and J. S. Famiglietti, 2005: Evaluation of 10 methods for initializing a land surface model. *J. Hydrometeor.,* **6,** 146-155.

Skamarock, W. C., J. B. Klemp, J. Dudhia, D. O. Gill, D. M. Barker, M. G. Duda, X-Y. Huang, W. Wang and J. G. Powers, 2008: A Description of the Advanced Research WRF Version 3, NCAR Technical Note, NCAR/TN–475+STR, 123 pp. [Available on-line at: http://www.mmm.ucar.edu/wrf/users/docs/arw_v3.pdf]

Zeng, X., R. E. Dickinson, A. Walker, M. Shaikh, R. S. DeFries, and J. Qi, 2000: Derivation and evaluation of global 1-km fractional vegetation cover data for land modeling. *J. Appl. Meteor.,* **39,** 826-839.

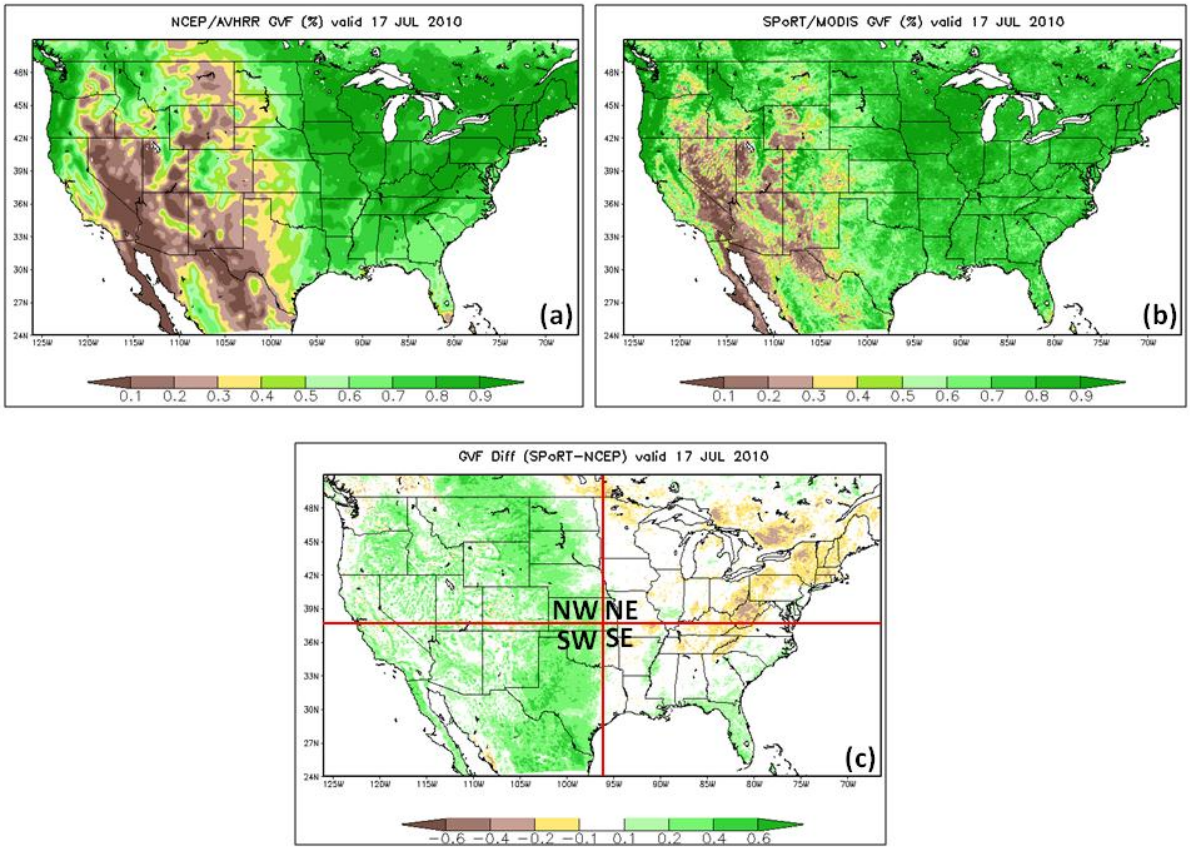

Figure 1. Comparison of the two GVF datasets and their differences on 17 July (a) NCEP GVF (b) SPoRT GVF and (c) differences between the datasets (SPoRT-NCEP). Panel c also shows the CONUS domain broken up into the four quadrants used for analysis.

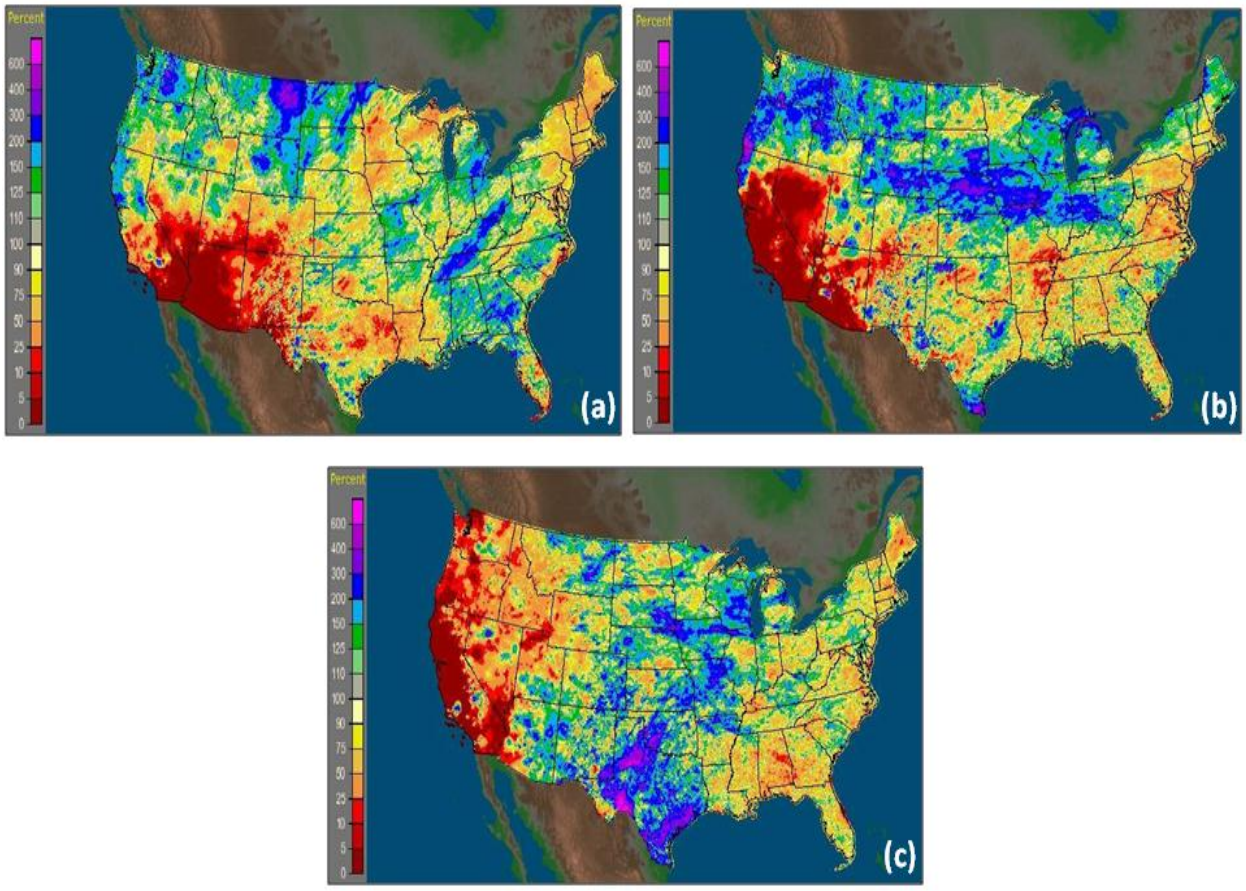

Figure 2. Observed precipitation departure from normal (in percent) during 2010 for the months of (a) May, (b) June, and (c) July.

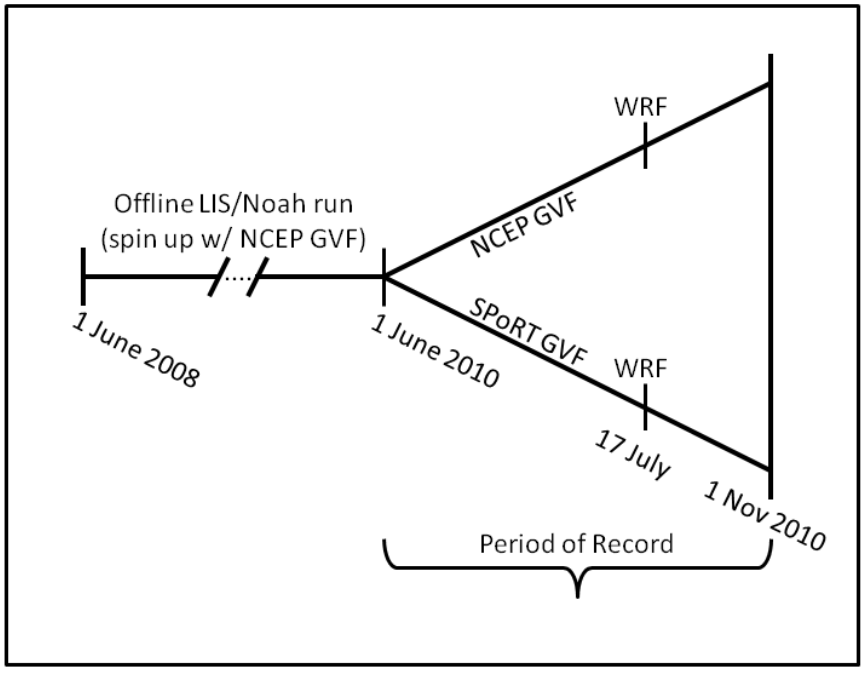

Figure 3. The above figure is a graphical representation of the methodology for the this experiment. The graphic shows how the spin up run was created and then ran until the two GVF datasets were compared. It also shows the date on which the WRF case study was conducted.

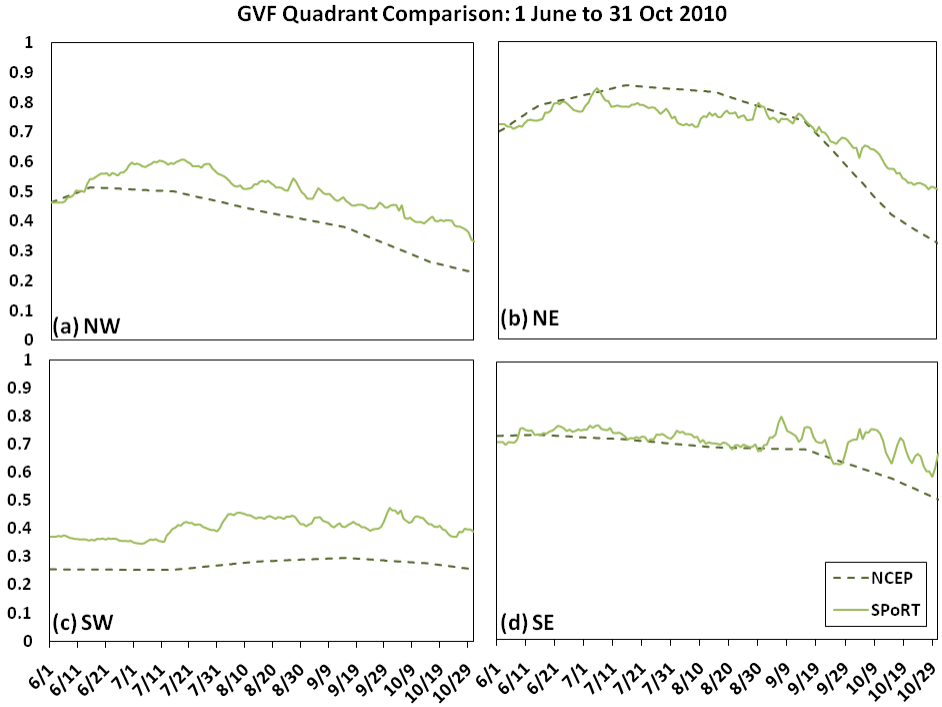

Figure 4. A daily comparison of the 2010 SPoRT GVF to the NCEP climatology, valid over the four quadrants depicted in Figure 1c: (a) Northwest, (b) Northeast, (c) Southwest, and (d) Southeast.

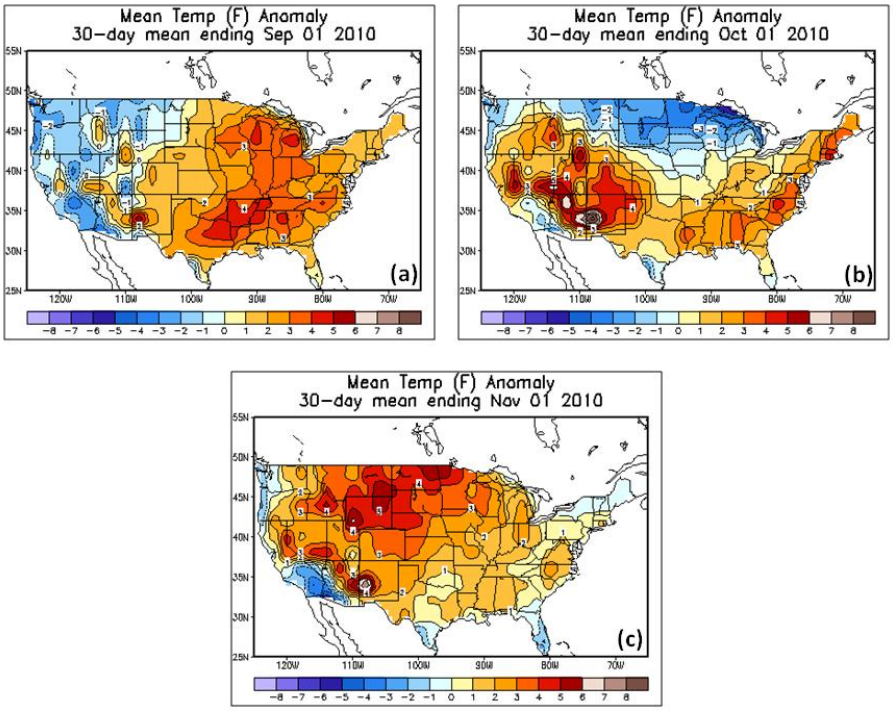

Figure 5. Average temperature anomalies for the 3-month span of August through October 2010: (a) August, (b) September (c) October.

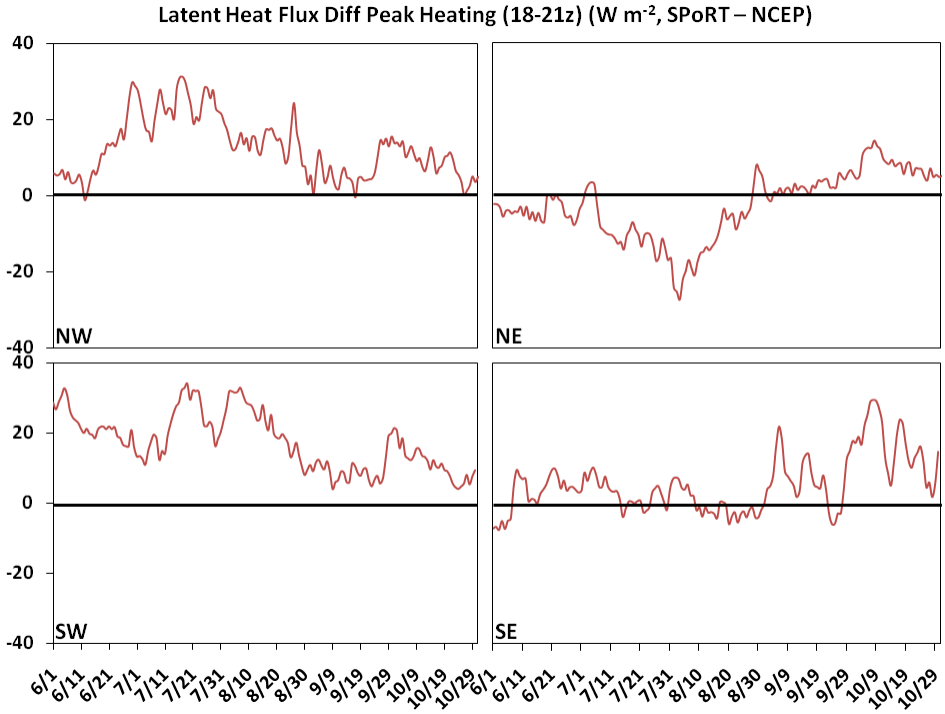

Figure 6. A daily comparison showing the difference between the 2010 SPoRT and the NCEP climatology average latent heat flux in LIS-Noah for the time period 1800–2100 UTC, valid over the four quadrants depicted in Figure 1c: (a) Northwest, (b) Northeast, (c) Southwest, and (d) Southeast.

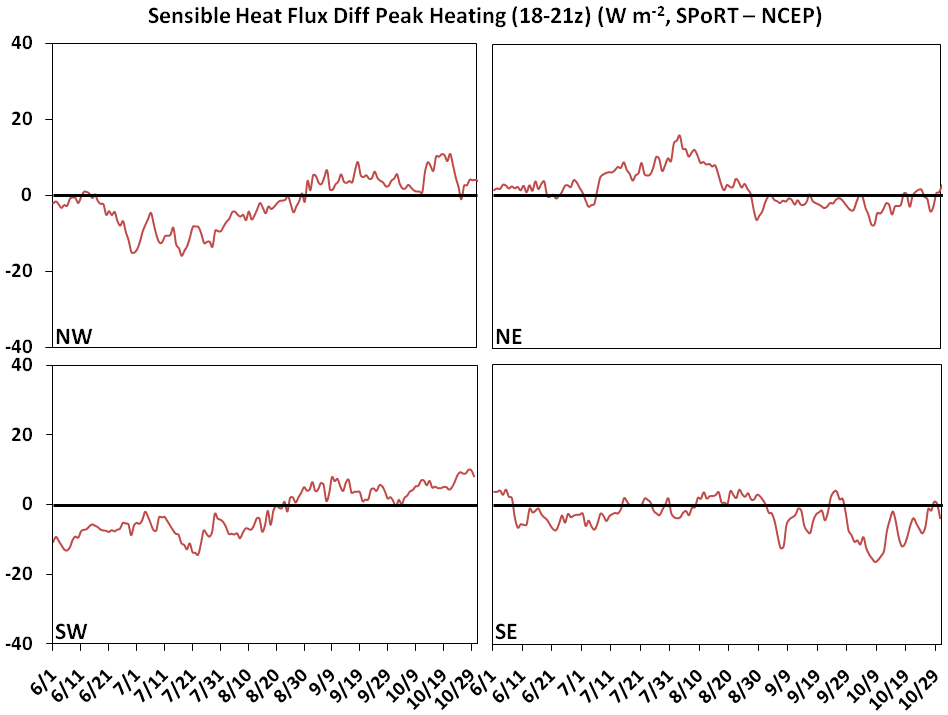

Figure 7. Same as in Figure 6, except for the average sensible heat flux difference.

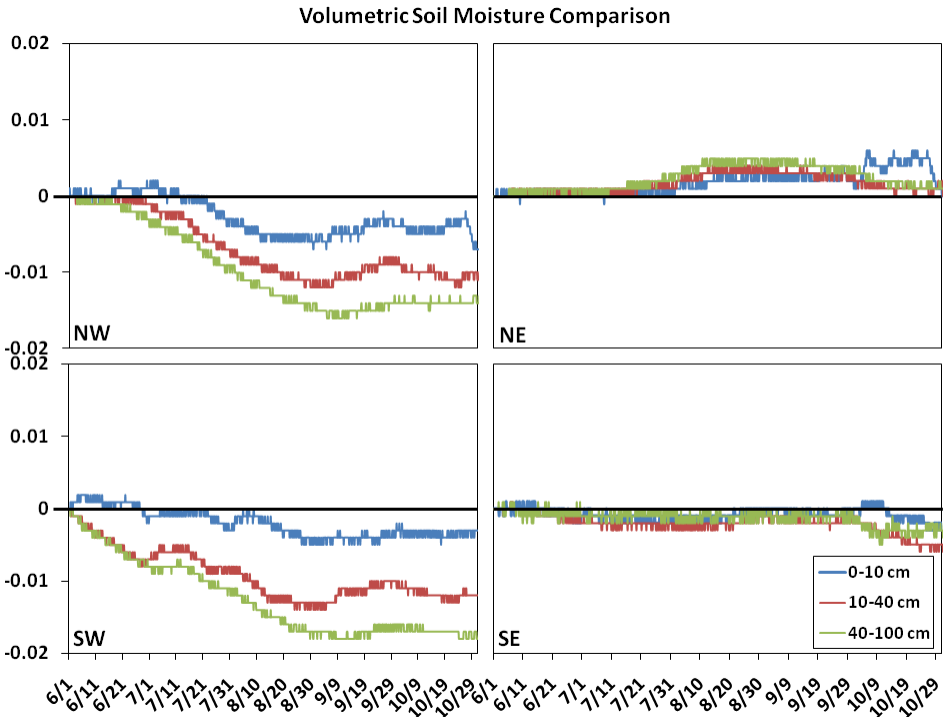

Figure 8. A comparison showing the difference in the 2010 SPoRT and the NCEP climatology volumetric soil moisture in LIS-Noah valid over the four quadrants depicted in Figure 1c: (a) Northwest, (b) Northeast, (c) Southwest, and (d) Southeast.

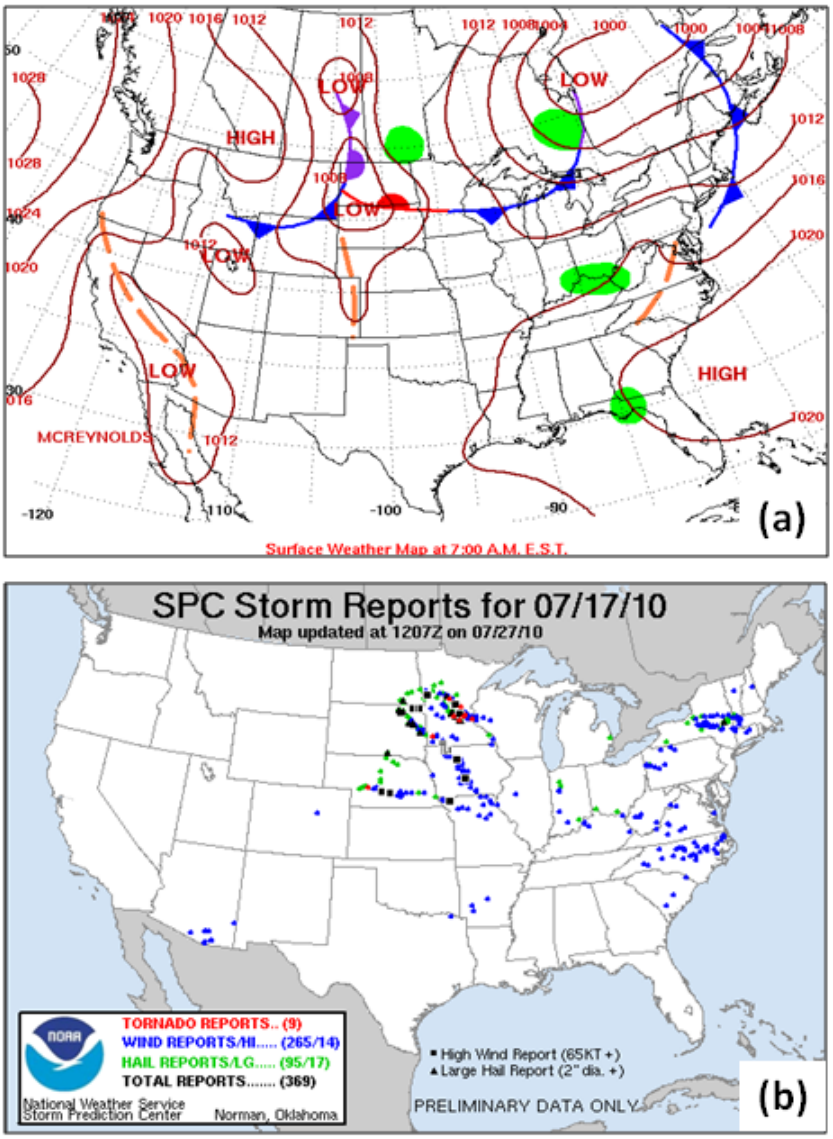

Figure 9. Overview of the 17 July 2010 severe weather event in the Upper Midwest. (a) The 1200 UTC surface analysis, and (b) Storm Prediction Center storm reports for 17 July 2010.

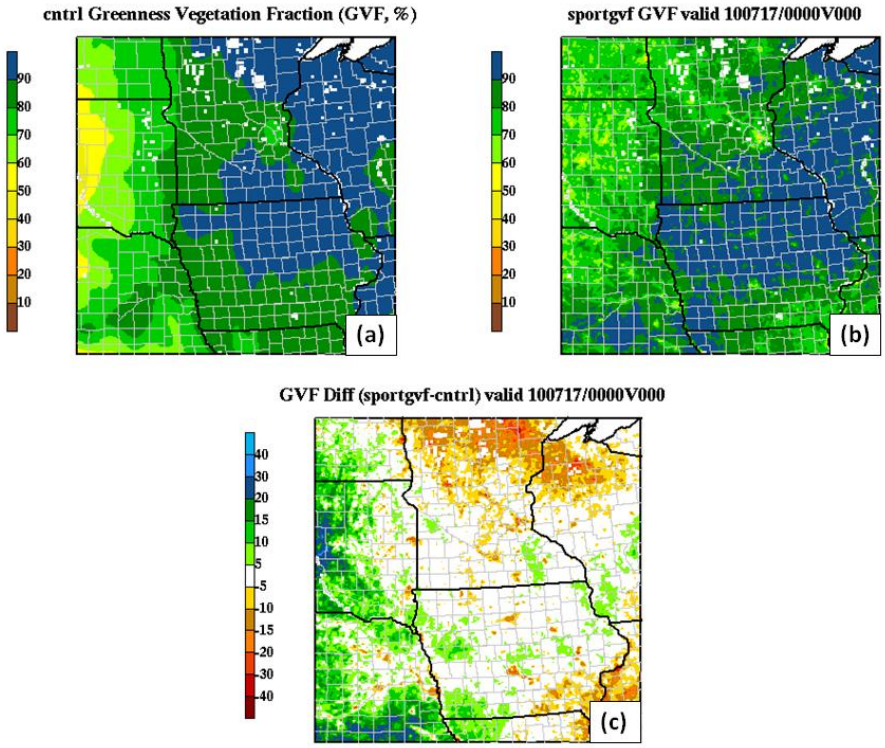

Figure 10. Greenness Vegetation Fraction (GVF) on the focus domain for the 17 July 2010 WRF simulations, depicting (a) NCEP GVF, (b) SPoRT GVF, and (c) the difference (SPoRT–NCEP).

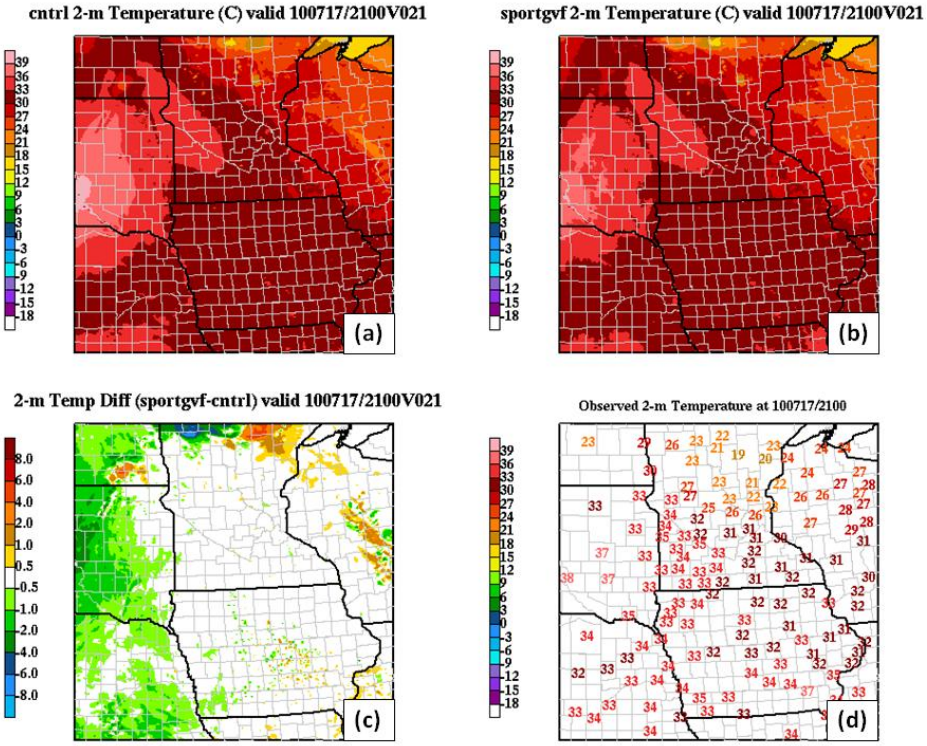

Figure 11. Simulated and observed 2-m temperatures valid at 2100 UTC 17 July 2010. Fields shown include (a) control WRF 21-h simulation using the NCEP GVF, (b) SPoRT-WRF 21-h simulation using MODIS GVF, (c) difference in WRF simulations (SPoRT–NCEP), and (d) observations.

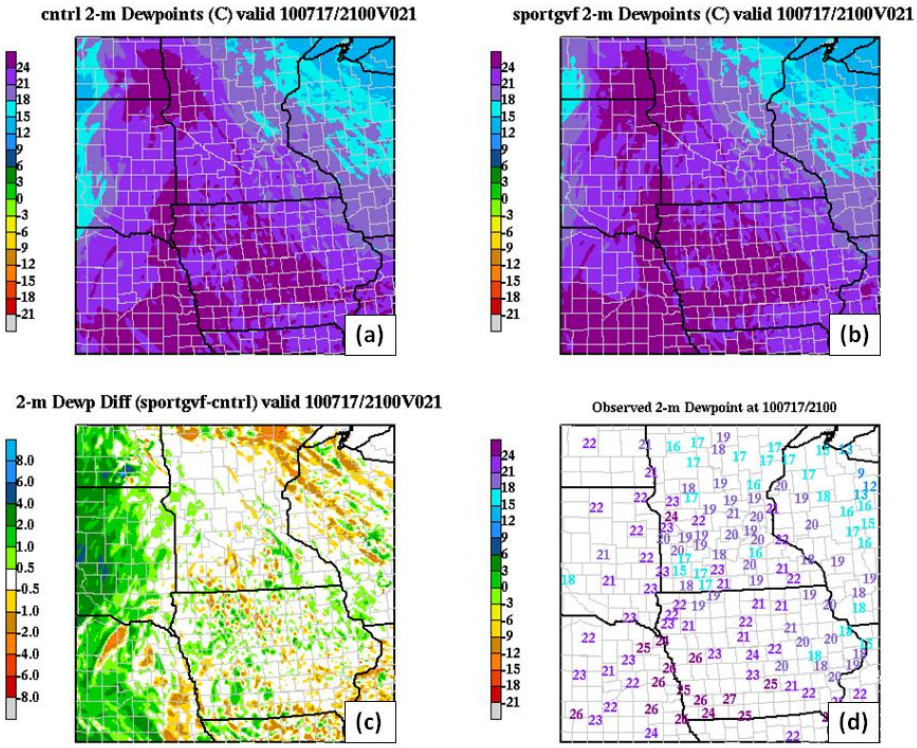

Figure 12. Same as in Figure 11, except for 2-m dewpoint.

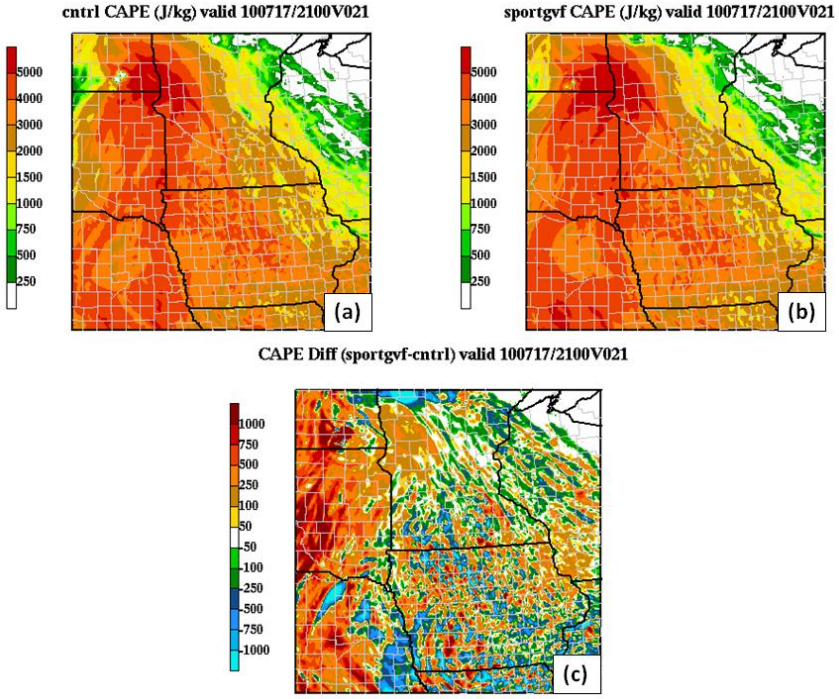

Figure 13. Convective Available Potential Energy (CAPE) for the 21-h forecast from the 0000 UTC WRF runs on 17 July 2010, showing (a) control WRF, (b) SPoRT-WRF, and (c) difference (SPoRT–control).

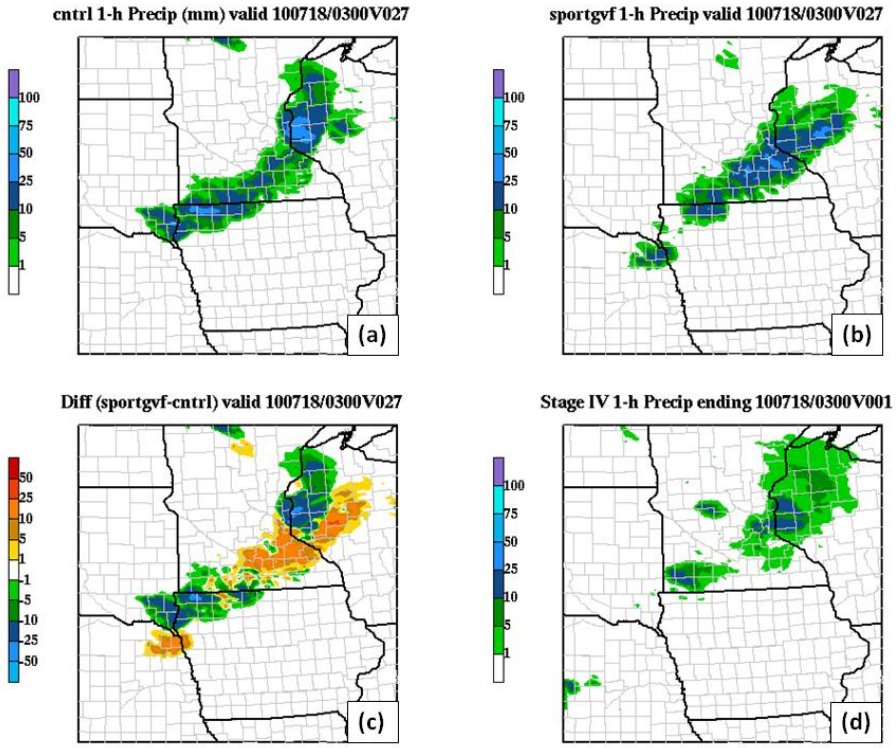

Figure 14. Simulated and analyzed 1-h accumulated precipitation (mm) for the hour ending 0300 UTC 28 July 2010, depicting the (a) 21-h control WRF forecast, (b) 21-h SPoRT-WRF forecast, (c) forecast difference (SPoRT–control), and (d) stage IV precipitation analysis.

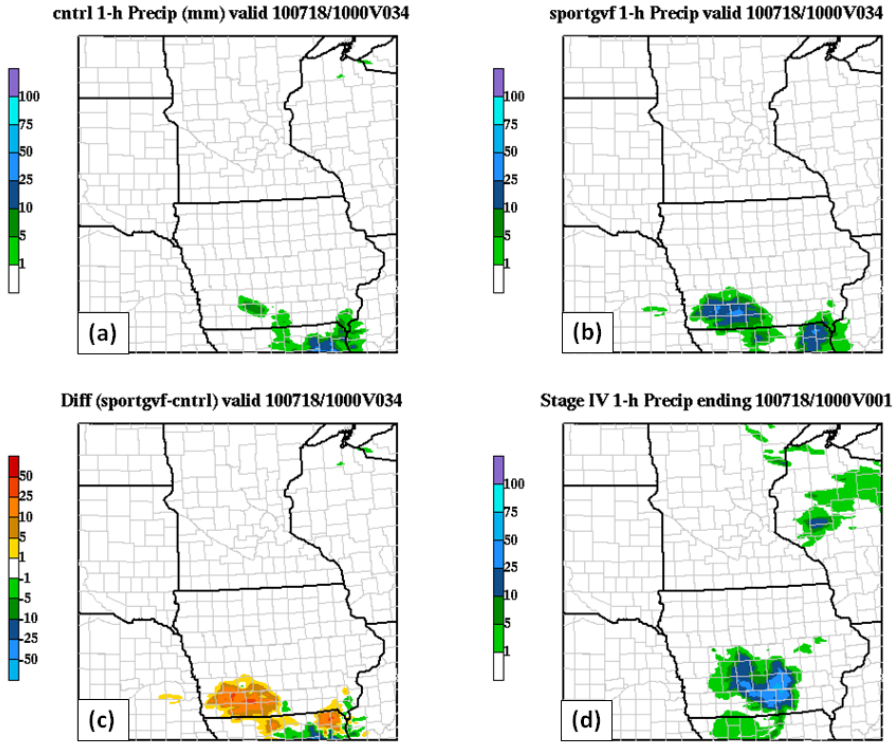

Figure 15. Same as in Figure 14, except for the hour ending 1000 UTC 28 July (34-h WRF forecasts).

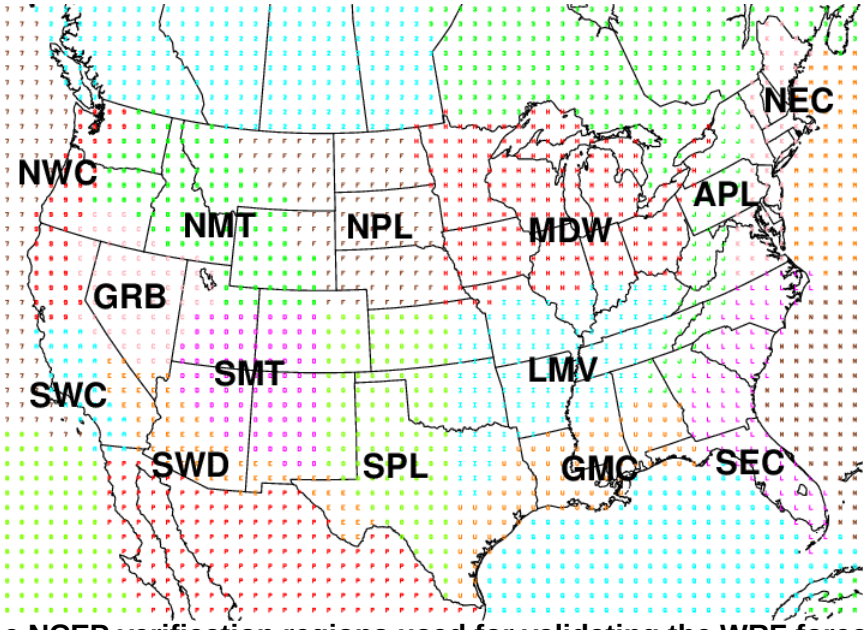

Figure 16. The NCEP verification regions used for validating the WRF forecasts from 17 July 2010. This experiment used the Midwestern (MDW) and the Northern Plains (NPL) regions.

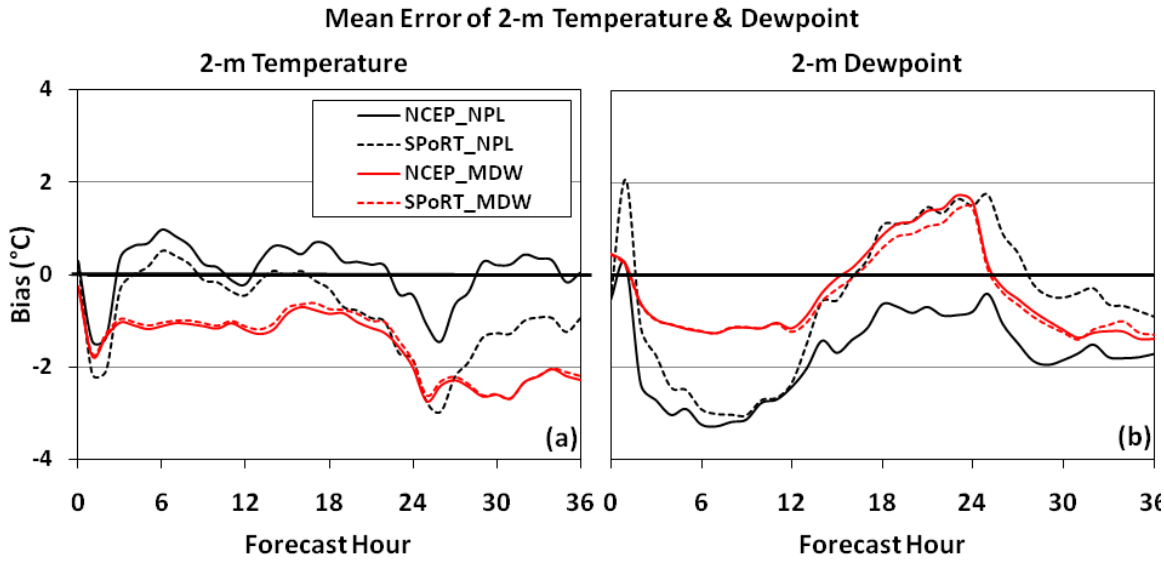

Figure 17. The mean error (bias) for the 17 July 2010 WRF forecast of (a) 2-m temperature, and (b) 2-m dewpoint.

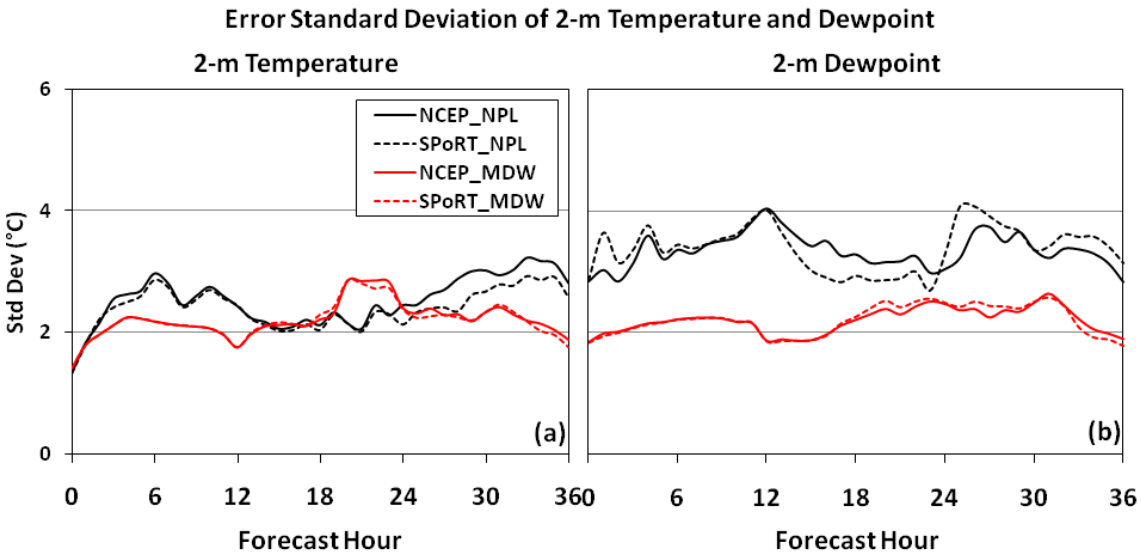

Figure 18. The error standard deviation for the 17 July 2010 WRF forecast of (a) 2-m temperature, and (b) 2-m dewpoint.

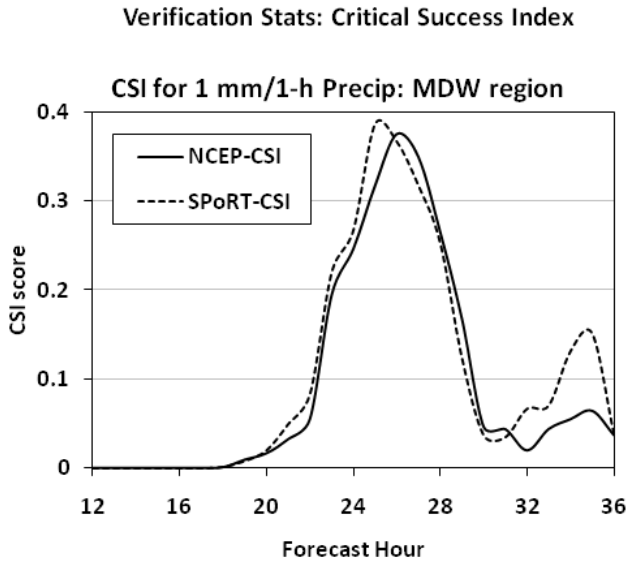

Figure 19. Critical Success Index (CSI) for the 1-mm per hour accumulated precipitation over the Midwestern verification region.